Lab on a Chip

PAPER

View Article Online
View Journal | View Issue

# Hydrogel bioprinted microchannel networks for vascularization of tissue engineering constructs†

Cite this: *Lab Chip*, 2014, **14**, 2202

Luiz E. Bertassoni,[abc] Martina Cecconi,‡[bc] Vijayan Manoharan,‡[bc] Mehdi Nikkhah,[bc] Jesper Hjortnaes,[bc] Ana Luiza Cristino,[bc] Giada Barabaschi,[bc] Danilo Demarchi,[d] Mehmet R. Dokmeci,[bc] Yunzhi Yang[e] and Ali Khademhosseini*[bcfgh]



Received 9th January 2014,
Accepted 6th May 2014

DOI: 10.1039/c4lc00030g

www.rsc.org/loc

Vascularization remains a critical challenge in tissue engineering. The development of vascular networks within densely populated and metabolically functional tissues facilitate transport of nutrients and removal of waste products, thus preserving cellular viability over a long period of time. Despite tremendous progress in fabricating complex tissue constructs in the past few years, approaches for controlled vascularization within hydrogel based engineered tissue constructs have remained limited. Here, we report a three dimensional (3D) micromolding technique utilizing bioprinted agarose template fibers to fabricate microchannel networks with various architectural features within photocrosslinkable hydrogel constructs. Using the proposed approach, we were able to successfully embed functional and perfusable microchannels inside methacrylated gelatin (GelMA), star poly(ethylene glycol-co-lactide) acrylate (SPELA), poly(ethylene glycol) dimethacrylate (PEGDMA) and poly(ethylene glycol) diacrylate (PEGDA) hydrogels at different concentrations. In particular, GelMA hydrogels were used as a model to demonstrate the functionality of the fabricated vascular networks in improving mass transport, cellular viability and differentiation within the cell-laden tissue constructs. In addition, successful formation of endothelial monolayers within the fabricated channels was confirmed. Overall, our proposed strategy represents an effective technique for vascularization of hydrogel constructs with useful applications in tissue engineering and organs on a chip.

## 1. Introduction

Vascularization represents one of the key challenges in tissue engineering.[1] Within engineered tissue constructs, cells must be sufficiently close (100–200 μm) to oxygen and nutrient supply,[2–4] delivered *via* uniformly distributed networks of blood vessels and capillaries to prevent the formation of a necrotic core.[5] Due to the slow rate of host-capillary invasion upon implantation,[6] functionality of tissue substitutes heavily relies on the development of vascular networks within tissue constructs. Similarly, perfusable microchannel networks embedded in cell-laden hydrogels are highly desirable for *in vitro* models of drug discovery and organ on a chip platforms.[7–10]

The process of engineering vascularized tissue constructs generally relies either on cell based strategies or fabrication of a network of microchannels.[7] Cell-based approaches primarily involve endothelial cells, often assisted by other cell types such as pericytes and stem cells, to form self-organized and stable capillaries embedded within constructs.[11–17] These processes, however, are usually slow, heavily depending on biological mechanisms such as cellular morphogenesis, recruitment of mural cells[18] and the fusion of intracellular vacuoles.[16] Furthermore, this strategy mostly remains restricted to relatively thin constructs.[12,19] Alternatively, the development of artificial microchannels depends on utilization of microfabrication techniques to form highly organized vascular networks. To date, a number of reports have used perfusable constructs fabricated *via* layer-by-layer assembly of hydrogels with microfabricated grooves or microchannels.[10,20–22] These methods, however, are generally restricted to planar footprints and depend on multiple polymerization steps, which result in undesirable interfaces within the engineered tissues.

[a] *Biomaterials Research Unit, Faculty of Dentistry, University of Sydney, Sydney, NSW 2010, Australia*
[b] *Center for Biomedical Engineering, Department of Medicine, Brigham and Women's Hospital, Harvard Medical School, Boston, MA 02139, USA. E-mail: alik@rics.bwh.harvard.edu*
[c] *Harvard-MIT Division of Health Sciences and Technology, Massachusetts Institute of Technology, Cambridge, MA 02139, USA*
[d] *Department of Electronics and Telecommunications, Politecnico di Torino, Torino 10129, Italy*
[e] *Department of Orthopaedic Surgery, Stanford School of Medicine, Stanford, CA 94305, USA*
[f] *Wyss Institute for Biologically Inspired Engineering, Harvard University, Boston, MA 02115, USA*
[g] *Department of Maxillofacial Biomedical Engineering and Institute of Oral Biology, School of Dentistry, Kyung Hee University, Seoul 130-701, Republic of Korea*
[h] *Department of Physics, King Abdulaziz University, Jeddah 21569, Saudi Arabia*
† Electronic supplementary information (ESI) available. See DOI: 10.1039/c4lc00030g
‡ Authors contributed equally.

A recent strategy for fabrication of well defined microchannels within engineered tissues has been based on bioprinting techniques to position sacrificial template materials, such as carbohydrate glass[23] and 'fugitive inks' of Pluronic F127[24–27] enclosed inside a hydrogel matrix. Upon bioprinting, these templates are dissolved *via* external stimuli, thus resulting in immediate formation of organized microchannels. Although bioprinting strategy exhibits several advantages in fabricating well defined microchannels compared to layer-by-layer assembly, the proposed bioprinted sacrificial template materials have been usually associated with cytotoxic reaction byproducts originating from template dissolution.[28,29] For instance, bioprinted sacrificial glass carbohydrate templates have been reported to require coating with poly(D-lactide-co-glycolide) to prevent osmotic damage to cells enclosed inside the hydrogel.[23] Similarly, highly concentrated Pluronic F127 has shown significant cytotoxic effects.[30] Therefore, there exists a need to develop novel bioprinting-based techniques to engineer functional vascular networks within hydrogel constructs for tissue engineering and organs on a chip applications.[19]

In this paper, we report a bioprinting-based strategy in which agarose, a naturally derived polysaccharide, is used as a permissive template material for vascularization of engineered hydrogel constructs. In the proposed strategy, agarose fibers are bioprinted with a well-defined and controlled three dimensional (3D) architecture. Then, a hydrogel precursor is casted over the bioprinted templates and subsequently photopolymerized. After gelation, the bioprinted agarose fibers do not adhere to the surrounding photocrosslinked hydrogels. Hence the bioprinted templates can be easily removed to form fully perfusable networks without any requirement for template dissolution (Fig. 1). Herein, we demonstrate the effectiveness of the proposed strategy in fabricating microchannel networks and microfluidics constructs in a wide variety of photocrosslinkable hydrogels commonly used for tissue engineering applications. Furthermore, we utilize cell-laden methacrylated gelatin (GelMA) hydrogels as a model platform to demonstrate the effectiveness of the proposed technique in the development of vascularized hydrogel constructs to support cellular viability, differentiation and overall tissue functionality.

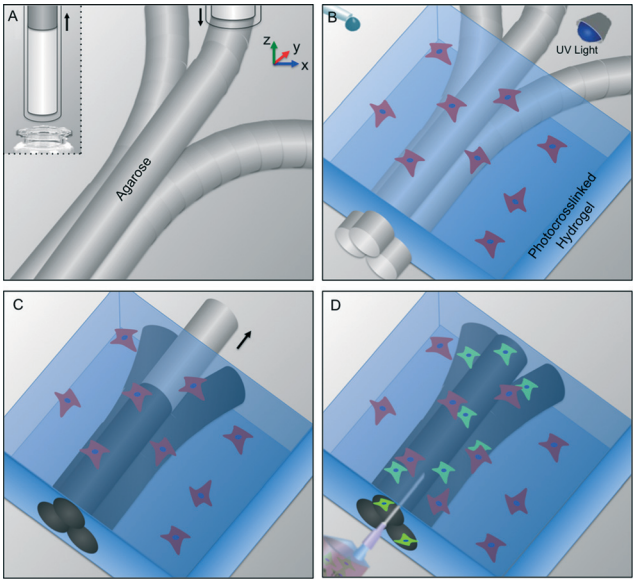


**Fig. 1** Schematic representation of bioprinting of agarose template fibers and subsequent formation of microchannels *via* template micromolding. a) A bioprinter equipped with a piston fitted inside a glass capillary aspirates the agarose (inset). After gelation in 4 °C, agarose fibers are bioprinted at predefined locations. b) A hydrogel precursor is casted over the bioprinted mold and photocrosslinked. c) The template is removed from the surrounding photocrosslinked gel. d) Fully perfusable microchannels are formed.

## 2. Materials and methods

### 2.1 Hydrogel preparation

GelMA, star poly(ethylene glycol-co-lactide) acrylate (SPELA), poly(ethylene glycol) dimethacrylate 1000 (PEGDMA), and poly(ethylene glycol) diacrylate 4000 (PEGDA) were used in this study. GelMA was synthesized as described previously.[31] Briefly, 10% (w/v) type A gelatin from porcine skin was mixed into Dulbecco's phosphate buffered saline (DPBS, Sigma) at 60 °C and stirred until fully dissolved. The degree of methacrylation of the resulting hydrogel, representative of the fraction of lysine groups reacted with methacrylate, was controlled by varying the amount of methacrylate present in the initial reaction mixture. To that end, 8% (v/v) methacrylic anhydride (Sigma) was added to the solution at a rate of 0.5 mL $min^{-1}$ and reacted for 3 h at 50 °C. A 5× dilution with additional warm (40 °C) DPBS was performed to stop the reaction, and the GelMA solutions were dialyzed using 12–14 kDa cutoff dialysis tubing against distilled water at 40 °C for one week. Finally, the solution was lyophilized for 3–4 days to generate a white porous foam that was stored at −80 °C until further use.

SPELA was synthesized based on a two-step procedure, following previously described protocols.[32] Primarily, star poly(ethylene glycol-co-lactide) (SPEL) was synthesized using melt ring-opening polymerization, where lactide and SPEG were polymerization initiators, and TOC was the reaction catalyst. SPEG was dried by azeotropic distillation from toluene prior to the reaction. The reactants were melted under dry nitrogen flow, TOC was added and the reaction was continued for 8 h at 135 °C. The product was dissolved in DCM, precipitated in ice cold methanol, followed by ether and hexane to remove unreacted monomers and vacuum-dried. In the following step, the resulting SPEL macromers were reacted with DCM and again dried by azeotropic distillation from toluene. After cooling in nitrogen, the macromere was dissolved in DCM and equimolar amounts of acryloyl chloride and TEA were added to limit the exothermic reaction, which proceeded for 12 hours. After the reaction, solvent was removed by vacuum distillation and the macromere redissolved in DCM and precipitated in cold ethyl ether. The reaction product was then dissolved in DMSO, dialyzed to remove

unreacted acrylic acid and the resulting SPELA was vacuum dried and stored for use.

For all experiments, 5 to 20% (w/v) GelMA, SPELA, PEGDMA and PEGDA were mixed with 0.5% (w/v) 2-hydroxy-1(4-(hydroxyethox)phenyl)-2-methyl-1-propanone (Irgacure, CIBA Chemicals) photoinitiator at 80 °C. Photopolymerization was performed by exposing GelMA and SPELA hydrogel precursors to UV light (360–480 nm) at 850 mW (Lumen Dynamics) (distance: 8.5 cm, time: 30 s and 8 s, respectively). Alternatively, PEGDA and PEGDMA were photocrosslinked using 750 mW of UV light exposure (distance: 7.5 cm, time: 50 s).

### 2.2 Bioprinting of agarose templates and fabrication of microchannels

The agarose template material was prepared by mixing the agarose powder (Organovo) with DPBS at 80 °C at different concentrations ranging from 2 to 8% (w/v). At these concentrations, agarose forms a viscous solution that gels reversibly at temperatures below 32 °C. For fluorescent images of the bioprinted templates, fluorescent microbeads (Createx Colors) were mixed with the agarose precursor at 0.1 to 0.5% (v/v) concentrations.

The fabrication of microchannels utilized a template micromolding technique, as schematically depicted in Fig. 1. In brief, a bioprinter (NovoGen MMX™, Organovo) equipped with pumps and dispensing capillaries (250 μm, 500 μm and 1000 μm diameters) assembled in motor-driven X–Y–Z stages was used for the experiments in this work. Agarose (80 °C) was loaded to the bioprinter (Fig. 1A, inset) by immersing the glass capillary fitted with a motorized piston in a heated agarose vial. The upward movement of the piston aspirated the agarose into the capillary. Next, the loaded capillaries were immersed in DPBS at 4 °C for 10 s. The metallic piston was then pushed down against the gelled material while a custom script controlled the dispense speed (2 mm $s^{-1}$) and the coordinated movement of the motorized X–Y–Z stages (Fig. 1A), as described previously.[33] After bioprinting, hydrogel precursors of GelMA, SPELA, PEGDMA and PEGDA were casted to fully cover the template fibers, photocrosslinked using UV light (Fig. 1B) and immersed in DPBS for 10 s. Interestingly, the agarose fibers did not adhere to the surrounding photocrosslinked hydrogels, hence the template fibers could be immediately aspirated with a light vacuum (ESI† movie 1) or removed *via* manual pulling (ESI† movie 2). Immediately after template removal (Fig. 1C), fully perfusable microchannels were formed (Fig. 1D). Furthermore, although the bioprinted fibers closely touched one another at intersection points, the fact that they were individually gelled before bioprinting ensured that they could be individually aspirated with ease.

To determine the reproducibility of microchannel formation relative to different hydrogels, 500 μm templates were bioprinted ($n$ = 6) and casted with GelMA, SPELA, PEGDMA and PEGDA precursors at concentrations ranging from 5 to 20% (w/v). Microchannel formation was deemed reproducible if all templates were successfully removed from the hydrogel constructs.

### 2.3 Mechanical properties

Preliminary observations suggested that slight elastic deformation of the surrounding photocrosslinked matrix was required for template removal (ESI† movie 2). Therefore, we investigated the elastic modulus of all hydrogels used in this study. For mechanical testing, 80 μL of hydrogel precursors of GelMA, SPELA, PEGDMA, and PEGDA, from 5 to 20%, were pipetted in a circular PDMS mold of 8 mm in diameter ($n$ = 6). Samples were photocrosslinked, retrieved from the molds and stored in DPBS for 3 h at room temperature. The discs were compressed at a rate of 1 mm $min^{-1}$ on a universal mechanical testing machine (Instron 5542). The compressive modulus was determined as the slope of the linear region corresponding to 0%–10% strain.

### 2.4 Swelling properties

Hydrogel swelling was expected to lead to slight constriction of the microchannels lumen, thus potentially preventing template removal. Therefore, we characterized the swelling properties of all hydrogels. Swelling analysis was performed in samples as prepared above. Samples were stored in DPBS for 24 h at room temperature. Gels were removed from DPBS, excess water was removed, and the swollen weight was recorded. Subsequently, the dry weight of polymer was recorded from the lyophilized samples and the mass-swelling ratio calculated as the ratio of wet mass to the mass of dry polymer ($n$ = 6).

### 2.5 Characterization of microchannels formation

To characterize the fabrication of different microchannel networks, bioprinted templates with linear, branching and lattice architectures were imaged in bright field using an inverted optical microscope (Nikon TE 2000-U). In addition, GelMA hydrogel constructs loaded with fluorescent microbeads (0.1% w/v) were imaged in fluorescence mode after fabrication of microchannels. To illustrate the interconnectivity of the fabricated network, a sequence of images was obtained while the channels were perfused with a 0.1% (v/v) solution of rhodamine-B. Additionally the constructs were imaged with the printed templates enclosed within and immediately after perfusing with a 0.1% (w/v) fluorescent microbead suspension using a digital camera (Nikon D3100).

### 2.6 Cell culture

We used mouse calvarial pre-osteoblasts cells (MC3T3) (ATCC) to evaluate the functionality of the microchannel networks in supporting cell viability and differentiation within the cell-laden hydrogel constructs. To study endothelial monolayer formation inside the bioprinted microchannels, green fluorescent protein (GFP)-expressing human umbilical vein endothelial cells (HUVECs) (ATCC) were used (passage 6 to 12). MC3T3s were cultured in $\alpha$-minimum essential medium ($\alpha$-MEM) supplemented with 10% (v/v) fetal bovine serum (FBS) and 1% (w/v) penicillin–streptomycin. To induce the differentiation of MC3T3s encapsulated in the hydrogels, 50 μg $ml^{-1}$ of ascorbic acid was added to the cell culture medium during culture of

 

cell-laden constructs. HUVECs were cultured in endothelial cell basal medium (EBM-2; Lonza) supplemented with endothelial growth kit (BulletKit, EGM-2; Lonza), maintained at 37 °C in a humidified, 5% $CO_2$-incubator. The media was changed 3 times per week and the cells were passaged once per week.

### 2.7 Cellular viability

Cell-laden hydrogel constructs were fabricated by dispensing 200 μl of a cell-laden GelMA hydrogel precursor ($5 \times 10^6$ cells $ml^{-1}$) on a PDMS mold (8 mm × 8 mm × 2 mm) with and without agarose template fibers of 1000 μm in diameter. Two parallel microchannels were fabricated following protocols described in section 2.1 and the cell-laden constructs were cultured in static conditions. Cell viability was determined by using a Live/Dead assay Kit (Invitrogen) according to the manufacturer's instructions. The number of live and dead cells was counted by ImageJ software using at least 4 images from different areas of 3 gels for each condition. The percentage of viable cells was then calculated based on the number of live cells divided by the total cell number.

### 2.8 Osteogenic differentiation

The effect of microchannels on the osteogenic differentiation of MC3T3 cells was assessed using a quantitative alkaline phosphatase (ALP) specific activity assay ($n$ = 3). Cell-laden hydrogels were washed twice with ultrapure water and preserved at −80 °C. Constructs were then thawed and mechanically lysed (Qiagen). The ALP activity was determined using a colorimetric $p$-Nitrophenyl Phosphate ($p$-NPP) method (Biocolor). The absorbance was measured at 405 nm after 1 hour of incubation at room temperature. ALP levels were then normalized to the amount of double-stranded DNA (dsDNA) as determined from a Pico Green assay (Invitrogen). For the Pico Green assay, 50 μl of working reagent was added to the 50 μl cell lysate of the sample. The sample was read at 485 nm excitation and 528 nm emission on a spectrophotometer (Biotek). The amount of dsDNA was calculated based on the standard curves of known dsDNA sample.

### 2.9 Endothelial monolayer formation

To form an endothelial monolayer, microchannels that were 250 μm, 500 μm and 1000 μm in diameter were fabricated in 10% w/v GelMA hydrogels and perfused with a cell suspension of $1.25 \times 10^6$ HUVECs ($n$ = 3) (ESI† movies 3A to C). The cell perfusion was repeated twice, and the constructs were flipped upside down in between each step. Cell-proliferation was quantified by counting the cellular nuclei at days 1, 3, and 7 at different fields of 5 individual regions within each microchannel.

### 2.10 Immunostaining of endothelial monolayers

After 7 days of culture, CD31 (PECAM-1) immunostaining was performed in vascularized hydrogel constructs to investigate the effective formation of an endothelial monolayer within the microchannels. For immunostaining the cells were fixed in 4% (w/v) paraformaldehyde for 30 min and soaked in 0.1% (v/v) Triton X-100 in DPBS for 30 min to permeabilize the cell membrane. Upon permeabilization, the samples were blocked in 10% (w/v) goat serum in DPBS for 1 h at room temperature and incubated in mouse anti-CD31 primary antibodies (Abcam) in 1/100 dilution. After three washes in DPBS, the hydrogels were incubated in 1/200 dilution of Alexa Fluor-594 conjugated goat anti-mouse secondary antibody (Abcam) for 6 h at room temperature (25 °C). Finally, samples were stained with DAPI (Sigma) and imaged using a confocal microscope (Nikon A1SiR). Constructs were cultured for up to 14 days, after which the endothelial monolayers were imaged inside microchannels and perfused with a fluorescent microbead suspension (0.1% w/v) to illustrate the functionality of the endothelialized channels.

### 2.11 Statistical analyses

Statistical analysis was performed using GraphPad Prism 6. Data are presented as the mean ± standard deviation. A comparison of values from different materials was carried out by one-way/two-way analysis of variance (ANOVA) followed by Tukey post-hoc tests.

## 3. Results and discussion

Despite significant advances in engineering complex tissues *in vitro*, there are still critical challenges for the development of vascular networks within engineered constructs.[1] Formation of vascular networks *in vitro* has been shown to facilitate the integration of tissue constructs with the host vasculature *via* rapid anastomosis.[4,34,35] Similarly, rapid fabrication of three dimensional microchannel networks in cell-laden hydrogels has widespread applications for *in vitro* models of drug discovery and organs on a chip platforms.[2,5,7,10,21] The primary objective of this study was to establish a new technique to fabricate microchannel networks within hydrogels for tissue engineering and organs on chip. In particular, a bioprinting strategy was utilized to generate 3D templates that readily formed microchannels upon removal from GelMA, SPELA, PEGDMA, and PEGDA hydrogels without any requirement for template dissolution. Furthermore, microchannels fabricated in cell-laden GelMA, allowed for enhanced mass transport in thick constructs, promoted high cellular viability and differentiation over time, and supported rapid formation of endothelial monolayers, thus representing an effective alternative for vascularization of hydrogel based engineered tissues and *in vitro* models of drug discovery.

### 3.1 Agarose template removal and microchannel formation

Agarose is a natural polysaccharide composed of repeating monomeric units of D-galactose and 3,6-anhydro-L-galactopyranose, forming a densely packed gel with low porosity *via* thermal-driven chain entanglements.[36] All of the surrounding hydrogels used in this study, on the other hand, were crosslinked *via* free-radical photopolymerization of acrylate groups, which did not form covalent chemical bonds with the agarose chains. Therefore, the lack of specific crosslinking

sites at the interface of the printed agarose fibers and the surrounding hydrogels may explain the easy removal of the template fibers. In particular, after casting and photocrosslinking GelMA, SPELA, PEGDMA and PEGDA precursors (surrounding hydrogels) over the bioprinted templates, the agarose fibers could be aspirated with a light vacuum (ESI† movie 1) or manually pulled out of the constructs with ease (ESI† movie 2), thus readily forming perfusable microchannel networks without the need for template dissolution. Therefore, the proposed technique prevented osmotic damage to encapsulated cells[23] or interactions of a dissolved template material that could modify the composition of the photocrosslinked matrix,[26,29] as reported previously. Interestingly, when agarose was mixed with the photocrosslinkable hydrogels before photopolymerization and then gelled, the resulting hydrogel was stable and no evident phase separation was present (ESI† Fig. S1).

We demonstrate that agarose templates at concentrations ranging from 2 to 8% could be successfully used to form microchannels in nearly all hydrogel concentrations, (5–20%, Fig. 2A). The only exception for successful microchannel formation was found for 20% PEGDA hydrogels (Fig. 2A). Since our preliminary observations suggested that slight deformation of the hydrogel matrix was required for template removal (ESI† movie 2), we expected that such limitation could be mainly due to the higher stiffness of 20% PEGDA compared to other hydrogels. In fact, we found that 20% PEGDA hydrogels had the highest elastic modulus (148.3 ± 28.9 kPa) of all groups tested ($p < 0.05$) (Fig. 2C). Moreover, results from mechanical testing (Fig. 2B and C) showed that the elastic modulus of all hydrogels increased gradually with an increase in polymer concentration, consistent with previous studies performed on GelMA hydrogels.[31,37] These findings suggest that there may exist a narrow threshold of elastic deformation (above 131.1 ± 14.9 kPa) at which the agarose template fibers could no longer be removed from the photocrosslinked hydrogels, thus hampering microchannel formation.

We further hypothesized that hydrogel swelling could lead to constriction of the microchannels and prevent template removal. However, our results showed that the higher hydrogel concentrations, including 20% PEGDA hydrogels, exhibited lower mass swelling ratios ($p < 0.001$) (Fig. 2D). These results discounted a relationship between hydrogel swelling and the ability to form microchannels. These findings were also consistent with previous reports showing an increase in mass swelling ratio for GelMA hydrogels combined with PEG[37] and hyaluronic acid.[38]

As the dimensions of native blood vessels vary from few millimeters in diameter down to tens of microns, successful vascularization strategies should allow for fabrication of channels with a wide range of diameters. Our results showed that microchannels with diameters ranging from approximately 1000 μm down to 150 μm could be readily fabricated (Fig. 2F and ESI† S2). Since the fibers were bioprinted individually, channels of different dimensions could be fabricated in the same construct (Fig. 2F) by using different dispensing capillaries. Furthermore, parallel overlapping of multiple template fibers over one another, allowed for fabrication of much larger channel diameters, as shown in Fig. 3B, 4A–Ai and B–Bi. In

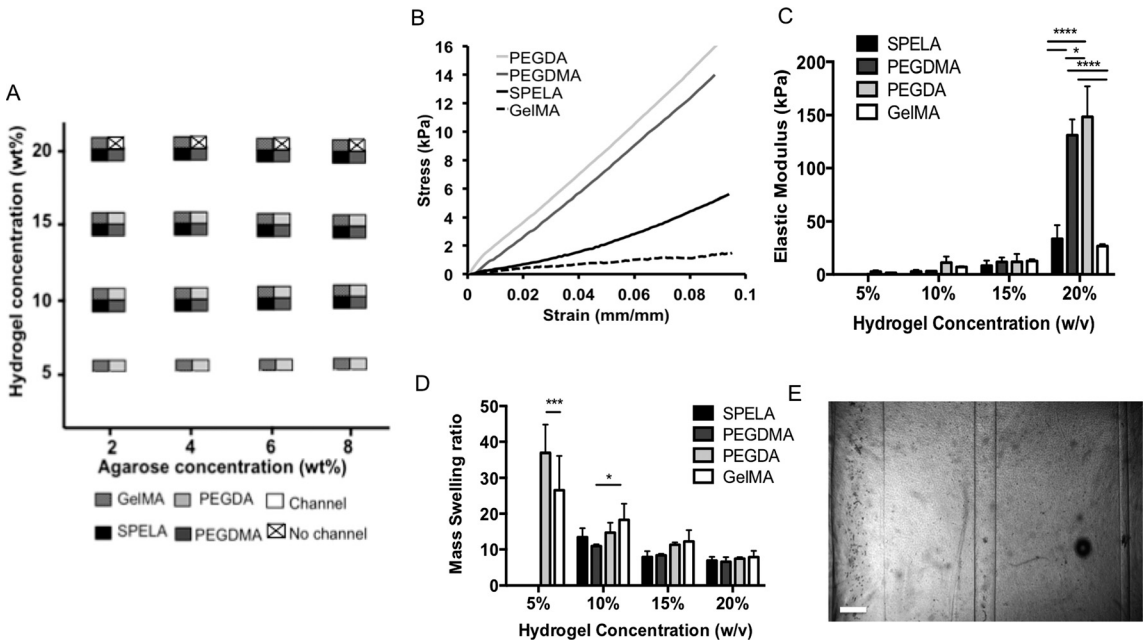


Fig. 2 Hydrogel properties associated with microchannel formation. a) Reproducibility of microchannel formation using 2 to 8% agarose templates in 5 to 20% GelMA, PEGDA, SPELA and PEGDMA hydrogels. Filled-squares represent successful microchannel formation, while crossed-squares represent failed microchannel formation. 5% PEGDMA and SPELA did not crosslink. b) Stress and strain response of hydrogels under compressive loading. c) 20% PEGDA hydrogels showed significantly higher modulus than 20% PEGDMA (*$p < 0.05$), 20% SPELA and 20% GelMA hydrogels (****$p < .0001$). d) 5% PEGDA hydrogels had higher mass swelling ratio than 5% GelMA hydrogels (***$p < 0.001$), while 10% GelMA hydrogels had a higher swelling ratio than PEGDMA hydrogels (*$p < 0.05$). e) Representative image of microchannels with approximately 1000 μm, 500 μm and 150 μm (left to right) in diameter are shown (500 μm scale bar).

 

these figures, the larger channels in the middle branched out into lateral individual channels of narrower diameters—a feature that is also observed in native vascular networks (Fig. 4A–Ai and B–Bi).

### 3.2 Architecture and morphology of microchannels

Microvascular networks are ubiquitous structures in biological systems. Emulating these structures in hydrogels *via* bioprinting technique is of considerable interest not only for tissue engineering and organs on a chip, but also for hydrogel microfluidics,[10,39,40] self-healing biomaterials[24,25,41] and organ printing.[33,42,43] The field of hydrogel microfluidics has gained increased attention in recent years.[21,44] The ability to explore cell behavior within 3D microenvironments under continuous flow condition has allowed researchers to explore physiologically relevant mechanisms in tissue-like microenvironments. For instance, in a recent study, a microfluidic device fabricated *via* soft lithography of collagen hydrogels was used to determine the association of inflammation with prothrombotic events in engineered blood capillaries.[18] A similar approach was used to reconstitute angiogenic sprouting morphogenesis *in vitro*.[45] Also, the mechanism of passive mass transport occurring in nephrons was recently recapitulated on a collagen hydrogel chip.[46] Despite significant progress, all of these approaches were limited by time-consuming microfabrication methods along with multiple polymerization steps to assemble microchannels. A major advantage of our bioprinting method is the ability to readily fabricate multiple microchannels in 3D arrangements, in a scalable manner, without any requirement for complex microfabrication process or template dissolution.

Fig. 3A and B demonstrate the versatility of the bioprinting method in fabricating linear and bifurcating templates, respectively, whereas Fig. 3C shows that more complex three dimensional grid architectures with overlapped Z-stacked fibers could also be dispensed to form template intersection points.[23] Linear printed fibers exhibited a preserved circular lumen (Fig. 3A-i and ESI† S3), while bifurcating (Fig. 3B-i) and lattice (Fig. 3C-i) configurations showed microchannel networks that integrated due to overlapping of the printed fibers (ESI† Fig. S4). The resulting microchannel junctions allowed for direct distribution of fluid throughout the entire scaffold even when perfused from a single inlet (Fig. 3D). To further confirm the network connectivity, a GelMA hydrogel microfluidic chip was fabricated by bioprinting two parallel template-lines on one plane, while an additional 'bridging' line was printed on a plane above, crossing over diagonally

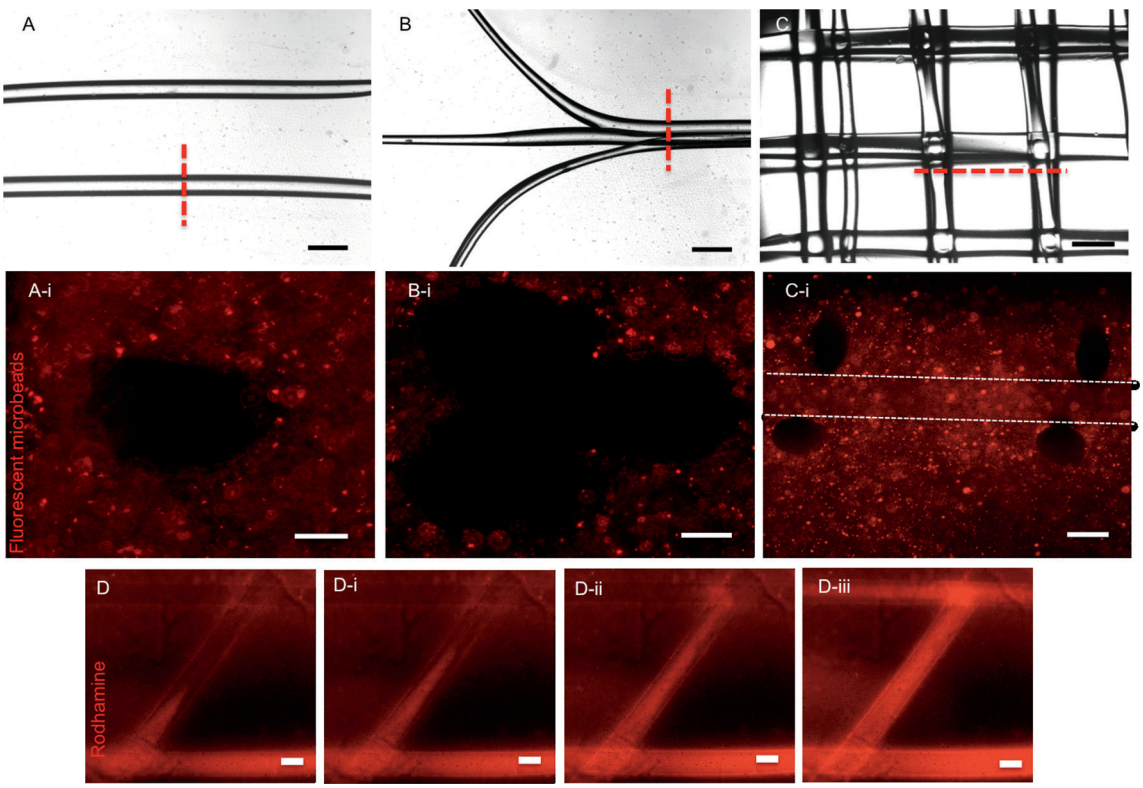


**Fig. 3** Bioprinted agarose template fibers and respective microchannels. a) Linear parallel agarose template fibers (scale bar 1 mm) and (a-i) cross-section (indicated by red dotted-line) perspective of a fluorescent microbead-laden GelMA hydrogel showing the circular shape of the lumen (scale bar 250 μm). Circular morphology of microchannels from additional gels is shown in ESI† Fig. S3. b) Planar bifurcating agarose template fibers (scale bar 1 mm) and (b-i) cross-section perspective (red dotted-line) of microbead-laden GelMA hydrogel microchannels showing the interconnectivity of the bifurcating network (scale bar 250 μm). Top view perspective of planar bifurcating network is shown in ESI† Fig. S4. c) Three dimensional lattice architecture of perpendicular bioprinted fibers (scale bar 1 mm) and (c-i) cross-section perspective (red dotted-line) of the network molded from lattice template. White lines indicate the upper and lower boundaries of the microchannel (scale bar 500 μm). d–diii) A sequence of images of a GelMA hydrogel chip with integrated microchannels perfused from one inlet (lower microchannel) illustrates the fluid flow through the entire construct (scale bar 500 μm).

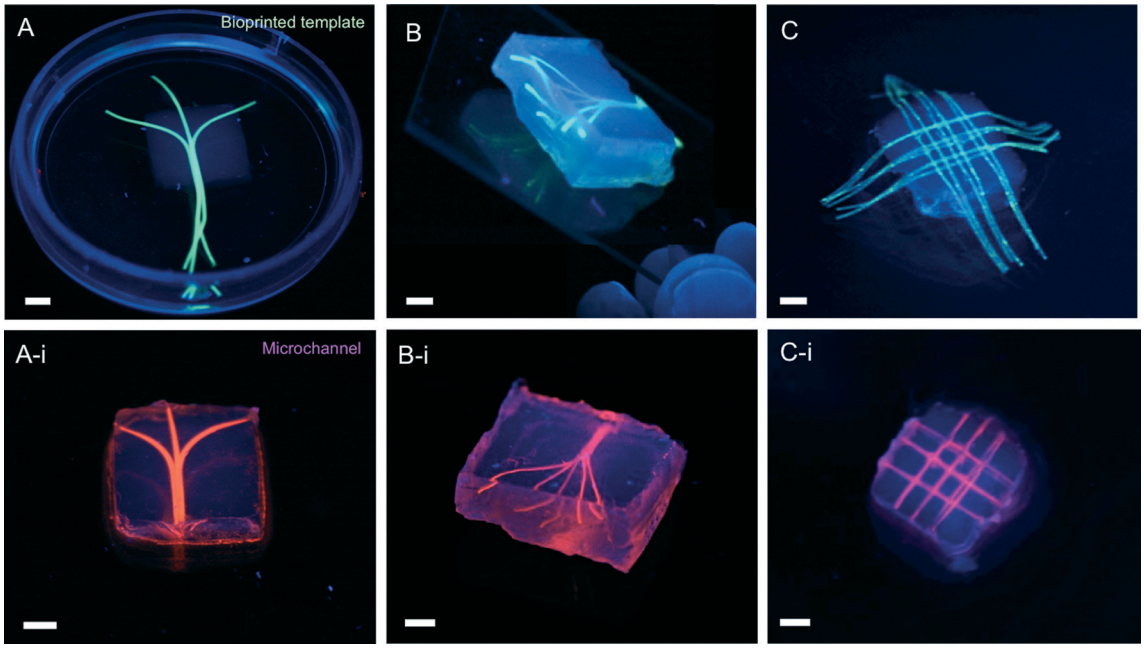


**Fig. 4** Photographs of the bioprinted templates (green) enclosed in GelMA hydrogels and the respective microchannels perfused with a fluorescent microbead suspension (pink). a) Planar bifurcating bioprinted templates in a GelMA hydrogel construct and (a-i) respective network after perfusion. b) 3d branching agarose templates embedded in a GelMA hydrogel construct and (b-i) resulting 3d branching network. c) 3d lattice template embedded in a GelMA hydrogel and (c-i) after perfusion. (scale bars 3 mm, microchannels have 500 μm in diameter).

(Fig. 3D). Upon perfusion of the hydrogel chip with a solution containing rhodamine dye from one inlet (bottom channel), the entire network was rapidly filled (Fig. 3D to D-iii). Such interconnection was further demonstrated in a more complex fluidic network in ESI† movie S4. A potential technical difficulty that needs to be considered in the proposed approach, however, is that the fabrication of microchannels requires each template to be individually aspirated or pulled from the crosslinked construct. This may prevent fabrication of more complex closed-loop networks.

In a recent work, it was demonstrated that GelMA promotes the formation of dense microvascular networks *via* self-assembly of endothelial and human mesenchymal stem cells *in vitro* and *in vivo*.[16] Furthermore, GelMA was shown to undergo transdermal photopolymerization leading to rapid integration with the host vasculature upon implantation.[47] Our bioprinting approach presented herein allowed for replication of architectures resembling branching microvascular networks either in a planar orientation (Fig. 4A and A-i) or in 3D architectures (Fig. 4B and B-i) with microchannels of relatively larger diameters (~100 μm to 1 mm). We argue, therefore, that the integration of larger channels, fabricated *via* the proposed bioprinting technique, with self-assembled microvascular networks in GelMA could ultimately lead to the formation of functional and vascularized tissue constructs with clinically relevant dimensions. A factor that needs to be considered for fabrication of larger constructs using photocrosslinkable hydrogels, however, is that the path length for UV light exposure will increase as the size of the construct increases. This eventually could lead to variable crosslinking properties throughout the thickness of the gel, restricting the effective size that constructs can be fabricated. We argue that recent strategies our group has developed enabling directed assembly of microgels, such as using programmable DNA glue[48] or 'Lego'-like interlocking of microstructural features in microfabricated microgels, for instance, represent effective solutions for this limitation.[49]

### 3.3 Functionality of cell-laden GelMA hydrogels with engineered microchannels

Before comparing the cellular viability between constructs with fabricated channels *versus* hydrogel blocks we determined the optimal concentration of GelMA hydrogels for MC3T3 proliferation upon encapsulation. Our preliminary results showed that higher hydrogel concentrations favored MC3T3 spreading and proliferation (ESI† Fig. S5). Therefore, subsequent experiments used 10% GelMA hydrogels.

To demonstrate the efficiency of our bioprinted microchannels to form cell-laden tissue constructs with improved functionality, we compared the viability of MC3T3 cells encapsulated in hydrogels with and without bioprinted microchannels. Our findings confirmed that GelMA hydrogels embedded with microchannels had significantly higher cellular viability at day 1 ($p < 0.05$) (Fig. 5C and E) and day 7 ($p < 0.0001$) (Fig. 5D and E) of culture. Hydrogel blocks (without microchannels) on day 7, on the other hand, showed only 60% cell viability (Fig. 5A, B and E). We further hypothesized that the presence of microchannels within the cell-laden constructs would lead to significantly higher differentiation of MC3T3s, as determined by the ALP activity levels, which was confirmed by the higher ALP levels detected in cell-laden hydrogels with microchannels on day 14 ($p < 0.0001$)

 

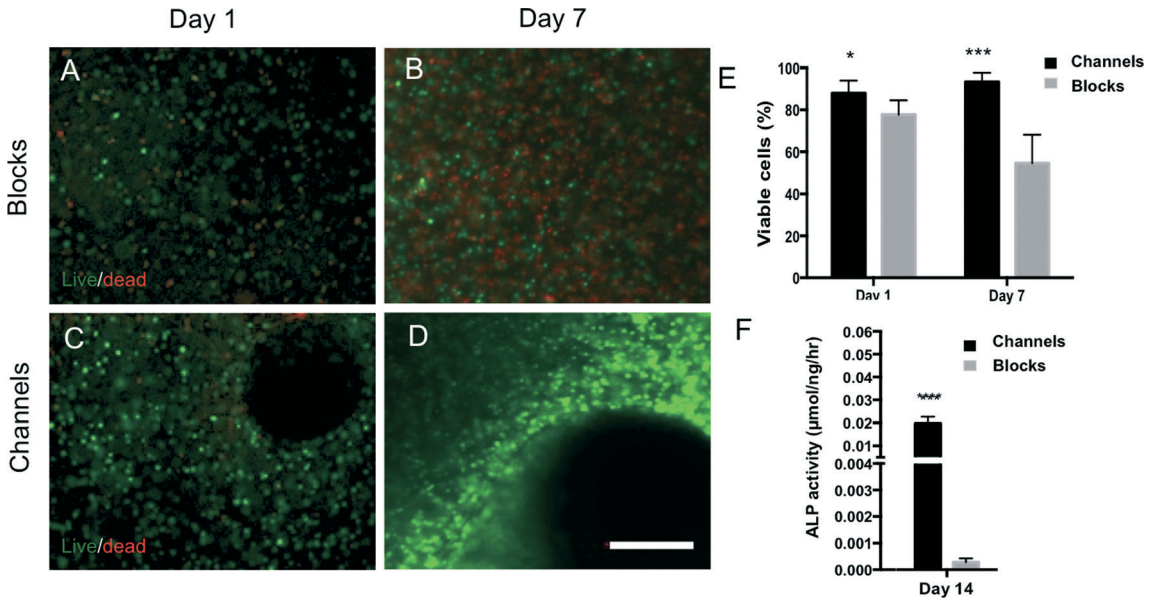


**Fig. 5** Viability and differentiation of MC3T3 cells encapsulated in 10% GelMA hydrogels comparing constructs with fabricated microchannels *versus* blocks without microchannels. Live and dead images of GelMA hydrogel blocks (a and b) and hydrogels with fabricated microchannels (c and d) at days 1 and 7. e) Hydrogel blocks had significantly lower viability at day 1 ($*p < 0.05$) and day 7 ($***p < 0.001$). f) ALP specific activity assay showed significantly higher ALP activity levels in cell-laden constructs with microchannels *versus* cell-laden hydrogel blocks on day 14 ($****p < 0.0001$). (scale bar 700 μm).

(Fig. 5F). Collectively, these results suggest not only that the fabricated channels allowed for improved nutrient transport preserving cell viability, but also promoted increased differentiation of encapsulated osteogenic cells. These observations were consistent with previous studies on vascularized cell-laden hydrogels fabricated *via* self-assembly of endothelial cells, enhancing the overall tissue functionality *in vitro*. For instance, in a recent study, encapsulation of HUVECs and 10T1/2 cells in PEG hydrogels resulted in microvascular formation and significantly decreased cell apoptosis over a course of 96 hours.[19] Similarly, in another study, hepatocyte-laden PEG hydrogels with fabricated microchannels lead to higher viability, albumin and urea production.[23] Therefore, our results are consistent with previous findings demonstrating that vascularized cell-laden tissue constructs can sustain improved tissue functionality *in vitro* over a long period of culture time.

### 3.4 Endothelial monolayer in GelMA hydrogel microchannels

Prior to studying the formation of an endothelial monolayer inside the lumen of the fabricated microchannels, we studied the proliferation of HUVECs seeded on flat GelMA hydrogel substrates at concentrations of 5, 7 and 10% (w/v).[31] Higher GelMA hydrogel concentrations favored HUVEC proliferation (ESI† Fig. S6). Therefore, 10% GelMA was selected for further studies on endothelial monolayer formation. We further investigated the feasibility of the fabricated microchannel networks to promote the formation of endothelial monolayers inside GelMA hydrogel constructs (Fig. 6A to K). Interestingly, HUVECs seeded within larger microchannels (1000 μm and 500 μm) reached a higher cell number in a significantly shorter amount of time as compared to ($p < 0.01$) narrower channels (250 μm) (Fig. 6A). The difference in the cell number, particularly in 1000 μm microchannels, was not significant between day 1 and day 7 of culture (Fig. 6A). Detailed observations (ESI† movie 3A to C) indicated that the cell perfusion in 250 μm microchannels was less effective than 500 μm and 1000 μm channels. This was mainly attributed to the difficulty to position the perfusion needle inside the narrower microchannels. Hence, the lower number of HUVECs within narrower microchannels overtime (Fig. 6A) was primarily due to the lower cell-seeding density, rather than specific geometric effects.[17] Despite the lower cell number in the 250 μm diameter microchannels, by day 7 of culture all channel geometries showed effective cell coverage within the inner surface of the channels (Fig. 6B–D). After 14 days of culture, the endothelial layers could be visualized by naked eye covering the entire length of the channels (Fig. 6E and ESI† S7A to D).

Fig. 6F to K show representative confocal and fluorescent images of immunostained HUVECs forming a confluent monolayer in a 500 μm diameter microchannel. These results were further confirmed by 3D projected images generated from z-stacked confocal images of endothelialized channels (ESI† movie 5A to E). High expression of CD31 marker (Fig. 6F, G and J) demonstrated the formation of cell-cell junctions, detected through high magnification fluorescent images (Fig. 6G). Similarly, representative 3D reconstructions of merged DAPI (ESI† movie 5A), CD31 (ESI† movie 5B) and GFP (ESI† movie 5C) fluorescent images, both from longitudinal (Fig. 6H) and cross-sectional (Fig. 6H, inset) views, showed a confluent lining of cells within the inner surface of the channels (ESI† movie 5D and E). Despite the formation of an endothelial lining, these constructs remained fully perfusable (ESI† movie 6) confirming the effective vascularization of GelMA hydrogel constructs *via* the proposed bioprinting technique.

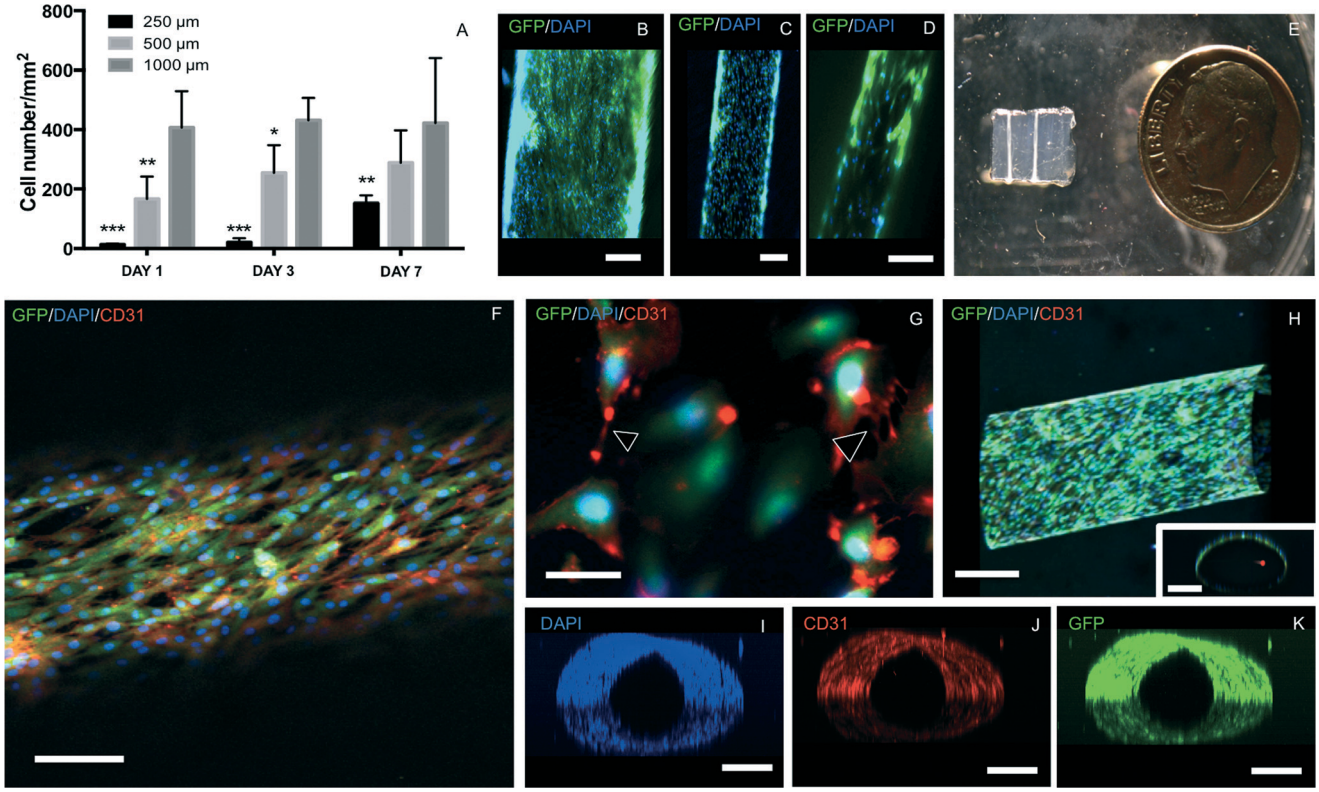


**Fig. 6** Representative confocal and fluorescent microscopy images of immunostained HUVECs forming a monolayer inside microchannels of different diameters after 7 days. a) Proliferation of HUVECs in 250 μm, 500 μm compared to 1000 μm channels (***$p < 0.001$, **$p < 0.01$ and *$p < 0.05$). b) 1000 μm, (c) 500 μm and (d) 250 μm microchannels lined with endothelial cells (scale bars 250 μm). e) Photograph of vascularized GelMA hydrogel construct with mature endothelial monolayer visible by naked eye covering the entire length of the channels. f) Confocal image of GFP/DAPI/CD31 markers from a HUVEC monolayer inside a 500 μm channel (scale bar 250 μm). g) Higher magnification fluorescence image of DAPI- and CD31-stained GFP-expressing HUVECs illustrating the cell–cell interactions (arrowheads) along the endothelial monolayer (scale bar 50 μm). h) Longitudinal view of z-stacked confocal images of a HUVEC-lined microchannel. the inset shows a cross-section view of the channel (scale bars 250 μm). Perpendicular views of z-stacked (i) DAPI, (j) CD31 and (k) GFP markers are also shown to illustrate the complete lining of the microchannel lumen (scale bars 250 μm). Three dimensional animations of the respective still images are shown as ESI† movies 5a–e.

## 4. Conclusion

In summary, we present a method for fabrication of microchannel networks within a wide range of commonly used hydrogels for tissue engineering applications. As a proof of concept, we demonstrated that the fabricated microchannels resulted in improved mass transport, viability and differentiation of osteogenic cells in cell-laden GelMA hydrogels. Finally, our results confirmed that GelMA hydrogels supported effective maturation of fully perfusable microvascular networks of different architectures and geometries. We believe that the proposed technique may find useful applications in the development of vascularized constructs for tissue engineering, hydrogel microfluidics and other applications relevant to regenerative medicine and organs on a chip.

## Acknowledgements

The authors acknowledge funding from National Institutes of Health (NIH-AR057837, DE021468 to Y.Y.; HL099073, AI081534, EB02597, GM095906 to A. K.) and the Presidential Early Career Award for Scientists and Engineers (PECASE) to A. K. The authors gratefully acknowledge funding by the Defense Threat Reduction Agency (DTRA). The content is solely the responsibility of the authors and does not necessarily represent the official views of the awarding agency. L.E.B acknowledges funding from the Australian Research Council (DP120104837).

## References

1 H. Bae, A. S. Puranik, R. Gauvin, F. Edalat, B. Carrillo-Conde, N. A. Peppas and A. Khademhosseini, *Sci. Transl. Med.*, 2012, **4**, 1–10.
2 R. K. Jain, P. Au, J. Tam, D. G. Duda and D. Fukumura, *Nat. Biotechnol.*, 2005, **23**, 821–823.
3 M. W. Laschke, B. Vollmar and M. D. Menger, *Tissue Eng., Part B*, 2009, **15**, 455–465.
4 N. Asakawa, T. Shimizu, Y. Tsuda, S. Sekiya, T. Sasagawa, M. Yamato, F. Fukai and T. Okano, *Biomaterials*, 2010, **31**, 3903–3909.
5 M. Radisic, L. Yang, J. Boublik, R. J. Cohen, R. Langer, L. E. Freed and G. Vunjak-Novakovic, *Am. J. Physiol.*, 2004, **286**, H507–516.
6 E. R. Clark and E. L. Clark, *Am. J. Anat.*, 1939, 251–301.

 

7 Rational design and applications of hydrogels in regenerative medicine. N. Annabi, A. Tamayol, J. A. Uquillas, M. Akbari, L. E. Bertassoni, C. Cha, G. Camci-Unal, M. R. Dokmeci, N. A. Peppas and A. Khademhosseini, *Adv. Mater.*, 2014, **26**, 85–123.
8 H. Bae, H. Chu, F. Edalat, J. M. Cha, S. Sant, A. Kashyap, A. F. Ahari, C. H. Kwon, J. W. Nichol, S. Manoucheri, B. Zamanian, Y. Wang and A. Khademhosseini, *J. Tissue Eng. Regener. Med.*, 2012, 1–14.
9 Y. Du, M. Ghodousi, H. Qi, N. Haas, W. Xiao and A. Khademhosseini, *Biotechnol. Bioeng.*, 2011, **108**, 1693–1703.
10 Y. Ling, J. Rubin, Y. Deng, C. Huang, U. Demirci, J. M. Karp and A. Khademhosseini, *Lab Chip*, 2007, **7**, 756–762.
11 A. F. Black, F. Berthod, N. L'Heureux, L. Germain and F. A. Auger, *FASEB J.*, 1998, **12**, 1331–1340.
12 L. L. Chiu, M. Montgomery, Y. Liang, H. Liu and M. Radisic, *Proc. Natl. Acad. Sci. U. S. A.*, 2012, **109**, E3414–3423.
13 M. C. Peters, P. J. Polverini and D. J. Mooney, *J. Biomed. Mater. Res.*, 2002, **60**, 668–678.
14 W. M. Elbjeirami and J. L. West, *Tissue Eng.*, 2006, **12**, 381–390.
15 J. E. Leslie-Barbick, J. E. Saik, D. J. Gould, M. E. Dickinson and J. L. West, *Biomaterials*, 2011, **32**, 5782–5789.
16 Y. C. Chen, R. Z. Lin, H. Qi, Y. Yang, H. Bae, J. M. Melero-Martin and A. Khademhosseini, *Adv. Funct. Mater.*, 2012, **22**, 2027–2039.
17 M. Nikkhah, N. Eshak, P. Zorlutuna, N. Annabi, M. Castello, K. Kim, A. Dolatshahi-Pirouz, F. Edalat, H. Bae, Y. Yang and A. Khademhosseini, *Biomaterials*, 2012, **33**, 9009–9018.
18 Y. Zheng, J. Chen, M. Craven, N. W. Choi, S. Totorica, A. Diaz-Santana, P. Kermani, B. Hempstead, C. Fischbach-Teschl, J. A. Lopez and A. D. Stroock, *Proc. Natl. Acad. Sci. U. S. A.*, 2012, **109**, 9342–9347.
19 M. P. Cuchiara, D. J. Gould, M. K. McHale, M. E. Dickinson and J. L. West, *Adv. Funct. Mater.*, 2012, **22**, 4511–4518.
20 A. P. Golden and J. Tien, *Lab Chip*, 2007, **7**, 720–725.
21 N. W. Choi, M. Cabodi, B. Held, J. P. Gleghorn, L. J. Bonassar and A. D. Stroock, *Nat. Mater.*, 2007, **6**, 908–915.
22 L. S. Wray, K. Tsioris, E. S. Gil, F. G. Omenetto and D. L. Kaplan, *Adv. Funct. Mater.*, 2013, 3404–3412.
23 J. S. Miller, K. R. Stevens, M. T. Yang, B. M. Baker, D. H. Nguyen, D. M. Cohen, E. Toro, A. A. Chen, P. A. Galie, X. Yu, R. Chaturvedi, S. N. Bhatia and C. S. Chen, *Nat. Mater.*, 2012, **11**, 768–774.
24 C. J. Hansen, R. Saksena, D. B. Kolesky, J. J. Vericella, S. J. Kranz, G. P. Muldowney, K. T. Christensen and J. A. Lewis, *Adv. Mater.*, 2013, **25**, 96–102.
25 C. J. Hansen, S. R. White, N. R. Sottos and J. A. Lewis, *Adv. Funct. Mater.*, 2011, 1–7.
26 W. Wu, A. DeConinck and J. A. Lewis, *Adv. Mater.*, 2011, **23**, H178–183.
27 W. Wu, C. J. Hansen, A. M. Aragón, P. H. Geubelle, S. R. White and J. A. Lewis, *Soft Matter*, 2010, 739–742.
28 L. M. Bellan, T. Kniazeva, E. S. Kim, A. A. Epshteyn, D. M. Cropek, R. Langer and J. T. Borenstein, *Adv. Healthcare Mater.*, 2012, **1**, 164–167.
29 L. M. Bellan, M. Pearsall, D. M. Cropek and R. Langer, *Adv. Mater.*, 2012, **24**, 5187–5191.
30 S. F. Khattak, S. R. Bhatia and S. C. Roberts, *Tissue Eng.*, 2005, **11**, 974–983.
31 J. W. Nichol, S. T. Koshy, H. Bae, C. M. Hwang, S. Yamanlar and A. Khademhosseini, *Biomaterials*, 2010, **31**, 5536–5544.
32 S. Moeinzadeh, D. Barati, X. He and E. Jabbari, *Biomacromolecules*, 2012, **13**, 2073–2086.
33 L. E. Bertassoni, C. C. Cardoso, V. Manoharan, A. L. Cristino, S. N. Bhise, W. A. Araujo, P. Zorlutuna, N. E. Vrana, A. M. Ghaemmaghami, M. R. Dokmeci and A. Khademhosseini, *Biofabrication*, 2014, 1–10, DOI: 10.1088/1758-5082/6/2/024105.
34 M. F. Leong, J. K. Toh, C. Du, K. Narayanan, H. F. Lu, T. C. Lim, A. C. Wan and J. Y. Ying, *Nat. Commun.*, 2013, **4**, 2353.
35 A. Alajati, A. M. Laib, H. Weber, A. M. Boos, A. Bartol, K. Ikenberg, T. Korff, H. Zentgraf, C. Obodozie, R. Graeser, S. Christian, G. Finkenzeller, G. B. Stark, M. Heroult and H. G. Augustin, *Nat. Methods*, 2008, **5**, 439–445.
36 M. Maaloum, N. Pernodet and B. Tinland, *Electrophoresis*, 1998, **19**, 1606–1610.
37 C. B. Hutson, J. W. Nichol, H. Aubin, H. Bae, S. Yamanlar, S. Al-Haque, S. T. Koshy and A. Khademhosseini, *Tissue Eng., Part A*, 2011, **17**, 1713–1723.
38 G. Camci-Unal, D. Cuttica, N. Annabi, D. Demarchi and A. Khademhosseini, *Biomacromolecules*, 2013, **14**, 1085–1092.
39 N. Annabi, S. Selimovic, J. P. Acevedo Cox, J. Ribas, M. Afshar Bakooshli, D. Heintze, A. S. Weiss, D. Cropek and A. Khademhosseini, *Lab Chip*, 2013, **13**(18), 3569–3577, DOI: 10.1039/c3lc50252j.
40 B. G. Chung, K. H. Lee, A. Khademhosseini and S. H. Lee, *Lab Chip*, 2012, **12**, 45–59.
41 K. S. Toohey, N. R. Sottos, J. A. Lewis, J. S. Moore and S. R. White, *Nat. Mater.*, 2007, **6**, 581–585.
42 K. Jakab, B. Damon, A. Neagu, A. Kachurin and G. Forgacs, *Biorheology*, 2006, **43**, 509–513.
43 C. Norotte, F. S. Marga, L. E. Niklason and G. Forgacs, *Biomaterials*, 2009, **30**, 5910–5917.
44 S. Kim, H. Lee, M. Chung and N. L. Jeon, *Lab Chip*, 2013, **13**, 1489–1500.
45 D. H. Nguyen, S. C. Stapleton, M. T. Yang, S. S. Cha, C. K. Choi, P. A. Galie and C. S. Chen, *Proc. Natl. Acad. Sci. U. S. A.*, 2013, **110**, 6712–6717.
46 X. Mu, W. Zheng, L. Xiao, W. Zhang and X. Jiang, *Lab Chip*, 2013, **13**, 1612–1618.
47 R. Z. Lin, Y. C. Chen, R. Moreno-Luna, A. Khademhosseini and J. M. Melero-Martin, *Biomaterials*, 2013, **34**, 6785–6796.
48 Y. Du, E. Lo, S. Ali and A. Khademhosseini, *Proc. Natl. Acad. Sci. U. S. A.*, 2008, **105**, 9522–9527.
49 H. Qi, M. Ghodousi, Y. Du, C. Grun, H. Bae, P. Yin and A. Khademhosseini, *Nat. Commun.*, 2013, **4**, 2275.